Effect of losses on tunable high impedance surface

Céline Ha, Jean-François Pintos, Priscillia Daquin, Serge Bories

Effect of Losses on Tunable High Impedance Surface

Céline Ha
Univ. Grenoble Alpes
CEA, Leti
F-38000 Grenoble, France
celine.ha@cea.fr

Jean-François Pintos
Univ. Grenoble Alpes
CEA, Leti
F-38000 Grenoble, France
jean-francois.pintos@cea.fr

Priscillia Daquin
Antenna Department
Centre National d'Etudes Spatiales (CNES)
F-31000 Toulouse, France
priscillia.daquin@cnes.fr

Serge Bories
Univ. Grenoble Alpes
CEA, Leti
F-38000 Grenoble, France
serge.bories@cea.fr

***Abstract*—Reconfigurable metasurfaces for multi-functional antennas can be designed by using lumped electronic elements in each unit cell. However, those additional components may not have negligible losses and it may lead to substantial absorption by the metasurface. In this paper, the influence on the performances of a High Impedance Surface (HIS) is investigated after the introduction of lumped elements with a significant resistive part, between each unit cell. The ratio between the HIS unloaded quality factor Q_0 and the unit cell electrical length is proposed as a criterion to compare different unit cell designs, since it takes into account losses inside the structures. The relationship between the quality factor and the usual definition of HIS bandwidth is also investigated.**

Keywords—losses, frequency-agile HIS, quality factor, Q-factor, metasurface

I. INTRODUCTION

Low-profile and unidirectional radiating systems are interesting characteristics for antenna applications. High Impedance Surface (HIS) can be used as in-phase reflector instead of a metallic ground plane in order to enhance the radiation performance of the feed antenna. HIS are often characterized by various criteria such as: the operating frequency when the phase of the reflection coefficient (Φ_{ref}) is equal to 0° [1]-[3], the HIS bandwidth where -90°<Φ_{ref}<+90° [1]-[3] or the magnitude of the reflection coefficient (|Γ|) [4]. As the instantaneous bandwidth of the HIS is limited, a coefficient *R* is proposed in [5] and is defined by the ratio between the fractional bandwidth over the size of the unit cell. The *R* coefficient is applied on multiple HIS geometries and it allows to highlight wideband and/or compact unit cell.

The introduction of voltage-driven elements such as PIN diodes or varactors allows the tuning of the HIS operating frequency and thus enables multi-functional applications for antenna design: wideband design [4], absorption [6]-[7], beam scanning [8], polarization control [9] and so on. In practice, active components' resistive part cannot be neglected [3]. Therefore, the reflection coefficient magnitude may become relevant and can be modeled as losses inside the metasurface.

As the HIS can be represented by a parallel LC resonant circuit, the quality factor *Q* is an adequate parameter to assess losses of a resonant circuit [11]. The quality factor have been studied in order to design metamaterials and metasurfaces according to: loss tangent constraint for magnetic metamaterial [12], presence of a PMC-like effect (Φ_{ref} = 0°) for thin HIS [13], bandwidth and thickness for thin HIS substrate [7], power stored in frequency selective surface [14] and physical parameters on the reflection properties of a reflectarray [15]. For all the studies mentioned about the *Q*-factor, only dielectric and conductor losses were taken into account.

In this paper, the ratio between the unloaded quality factor Q_0 and the unit cell electrical length is proposed as a criterion to evaluate the tunable HIS performance when adding capacitors with a significant resistive part. In Section II, the equivalent circuit model of a lossy HIS with additional capacitors is presented. The unloaded quality factor Q_0 and loaded quality factor Q_L are then extracted and compared to the definition of the HIS bandwidth for lossless additional capacitors and lossy capacitors. In Section III, the Q_0-factor is applied to three different unit cells: a patch, a 4-armed intertwined square spiral and a 6-armed intertwined hexagonal spiral in the case of lossy metasurface with additional lossy components. Comparison will be made according to the unloaded quality factor Q_0, the reflection coefficient magnitude |Γ|, the modified *R* coefficient which is the ratio between the HIS bandwidth and the unit cell electrical length, inspired by [5], and the criterion Q_0 over the unit cell electrical length.

II. EQUIVALENT CIRCUIT MODEL

A lossy HIS can be modeled by a capacitor *C* in series with a resistance R_{se}, parallel to an inductor *L* in series with a resistance R_{Cu}, Fig. 1(a) [1]. R_{se} represents the dielectric loss and R_{Cu}, the conductor loss. To modify the resonant frequency of the circuit, a lossy capacitor with a capacitance C_s and its equivalent series resistance R_s is placed in parallel to the previous circuit, Fig. 1(a). Transmission lines formalism is used as the HIS is studied under plane wave with normal incidence. After some mathematical transformations, the model is equivalent to a parallel RLC circuit, with the well-known *Q*-factor formulas [11]:

$$Q = \omega \frac{average\ stored\ energy}{dissipated\ power} \tag{1}$$

$$Q = \frac{R_{tot}}{\omega_0 L_{tot}} = \omega_0 R_{tot} C_{tot} \tag{2}$$

with $\omega_0 = 1/\sqrt{L_{tot}C_{tot}}$ at the resonance.

$$L_{tot} = L \tag{3}$$

under the condition that $R_{Cu}^2/L\omega \ll 1$.

$$C_{tot} = C + C_s \tag{4}$$

under the condition that $\omega^2 R_{se}^2 C^2 \ll 1$ and $\omega^2 R_s^2 C^2 \ll 1$ if $R_s \neq 0$.

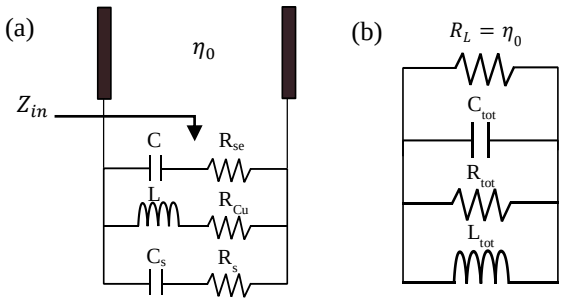

Fig. 1. Equivalent circuit model, in free space envrionnement, of (a) the lossy HIS with additional capacitor C_s under plane wave with normal incidence (b) the lossy HIS as a parallel RLC resonant circuirt connected to the external load R_L for the study of Q_L.

For $R_s = 0$,

$$\frac{1}{R_{tot}} = \frac{1}{R_1} + \frac{1}{R_2} \tag{5}$$

with

$$R_1 = \frac{1}{R_{se}C^2\omega^2} \tag{6}$$

under the condition that $\omega^2 R_{se}^2 C^2 \ll 1$.

$$R_2 = \frac{L^2\omega^2}{R_{Cu}} \tag{7}$$

under the condition that $R_{Cu}^2/L\omega \ll 1$.

For $R_s \neq 0$,

$$\frac{1}{R_{tot}} = \frac{1}{R_1} + \frac{1}{R_2} + \frac{1}{R_3} \tag{8}$$

with

$$R_3 = \frac{1}{R_s {C_s}^2 \omega^2} \tag{9}$$

under the condition that $\omega^2 R_s^2 {C_s}^2 \ll 1$.

The Q-factor defined here is a characteristic of the metasurface circuit itself and it is called the unloaded quality factor, Q_0. In practice, the metasurface is surrounded for instance by free space, and thus the influence of the environment can be modeled by the equivalent circuit of a parallel RLC circuit coupled to an external load resistor R_L equal to free space impedance η_0, Fig. 1(b). Thus, the HIS structure with its environment can be described as a loaded quality factor, $Q_{L,RLC}$, and it is related to Q_0 by [11]:

$$\frac{1}{Q_{L,RLC}} = \frac{1}{Q_0} + \frac{1}{Q_e} \tag{10}$$

with $Q_e = R_L/(\omega_0 L_{tot})$, the external quality factor.

For parallel RLC circuit,

$$Q_{L,RLC} = \frac{Q_0}{1 + R_{tot}/R_L}. \tag{11}$$

Q_0 is also related to half-power fractional bandwidth (FBW) of the resonator [11]:

$$FBW = {}^{1}/_{Q_0} \tag{12}$$

and the FBW is extracted from the input impedance magnitude $|Z_{in}|$, Fig. 1(a), versus the frequency, when $|Z_{in}|$ equals to $R_{tot}/\sqrt{2}$ for parallel RLC circuit.

The reflection coefficient Γ is defined as:

$$\Gamma = \frac{Z_{in} - \eta_0}{Z_{in} + \eta_0}. \tag{13}$$

III. Quality Factors and HIS Bandwidth of Square Patch

The geometry under study for the HIS is a square patches array on a grounded FR4 substrate (ε_r = 4.4, tanδ = 0.02), which height is h = 19.9 mm. The unit cell periodicity is D = 95.63 mm and the gap between patches is d = 2.5 mm, with copper as metallic conductor ($\sigma = 5.8 \times 10^7$ S/m) and with active lossy capacitor (C_s, R_s) between each adjacent unit cell, Fig. 2. The smallest hypothetical sphere enclosing the unit cell has a radius defined as a. The analytical formulas of L and C for this structure are available in [1] and [16] respectively. $Q_{L,RLC}$ of the HIS, Fig. 3, is compared to $Q_{L,\pm 90^\circ} = 1/FBW_{\pm 90}$, where $FBW_{\pm 90}$ is the fractional bandwidth of the infinite HIS, i.e. the ratio between the bandwidth of the HIS where $-90° < \Phi_{ref} < +90°$ and its operating frequency f_0. The HIS is analyzed with infinite boundary conditions and under plane wave with normal incidence. All the simulations are performed with the software Ansoft HFSS v2021R1 [17]. The value of capacitor C_p ranges from 1 pF to 60 pF and it enables to tune the HIS operating frequency f_0.

For lossless additional capacitors (R_s = 0 Ω), Fig. 3, it can be observed that $Q_{L,RLC}$ and $Q_{L,\pm 90^\circ}$ follow the same trend, whereas for lossy additional capacitors (R_s = 10 Ω), Fig. 4, this is not the case anymore. Therefore, $Q_{L,RLC}$ is not related to $FBW_{\pm 90}$ only, but it also takes into account the influence of additional losses from the capacitors. Furthermore, when the reflection coefficient phase does not cross 0°, for electric size a/λ_0 below 0.06, in Fig. 5(a), $Q_{L,RLC}$ is still defined in Fig. 4 whereas the HIS bandwidth definition is no longer valid. Fig. 5(b) shows the magnitude of the reflection coefficient $|\Gamma|$: as the operating frequency decreases, the losses inside the HIS seem to increase until the phase swing phenomenon at a/λ_0=0.06, from which point the losses inside the HIS seem to decrease as the operating frequency decreases. However, $Q_{L,RLC}$ is not consistent with the evolution of $|\Gamma|$ when the phase-swing phenomenon appears: as in (1) and (11), lower losses implies higher Q_0 and so a higher $Q_{L,RLC}$, meanwhile, $Q_{L,RLC}$ decreases when $|\Gamma|$ decreases.

Thus, in order to compare different designs of unit cells regardless of their environment, the unloaded quality factor Q_0 is proposed as a criterion. The Q_0 of the square patches array under study and the magnitude of the input impedance $|Z_{in}|$ are available in Fig. 6 and Fig. 7 respectively. The analytical Q_0 matches with the simulated Q_0. As the electrical length increases, the value of Q_0 also increases and it is consistent with the reduction of the FBW, Fig. 7.

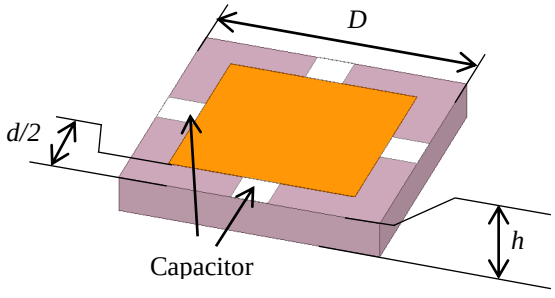

Fig. 2. HIS square patch with additional capacitors.

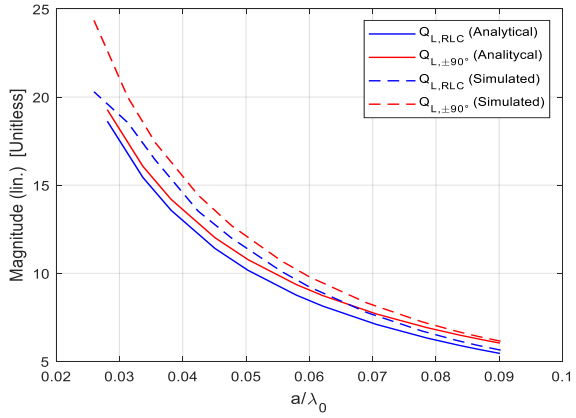

Fig. 3. Comparison between $Q_{L,RLC}$ (blue) and $Q_{L,\pm90^\circ}$ (red) for the square patch HIS with lossless additional capacitor (R_s = 0 Ω) and between analitycal (line) and simulated (dashed line) results.

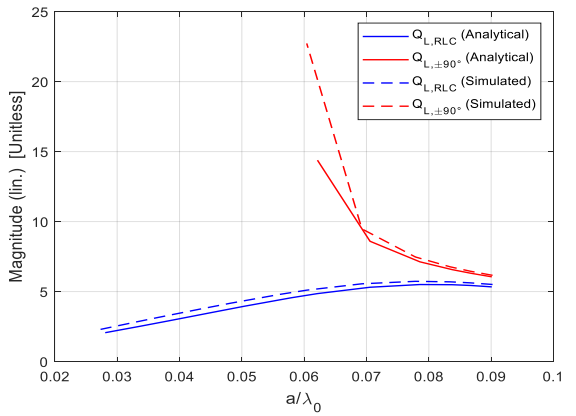

Fig. 4. Comparison between $Q_{L,RLC}$ (blue) and $Q_{L,\pm90^\circ}$ (red) for the square patch HIS with lossy additional capacitor (R_s = 10 Ω) and between analitycal (line) and simulated (dashed line) results.

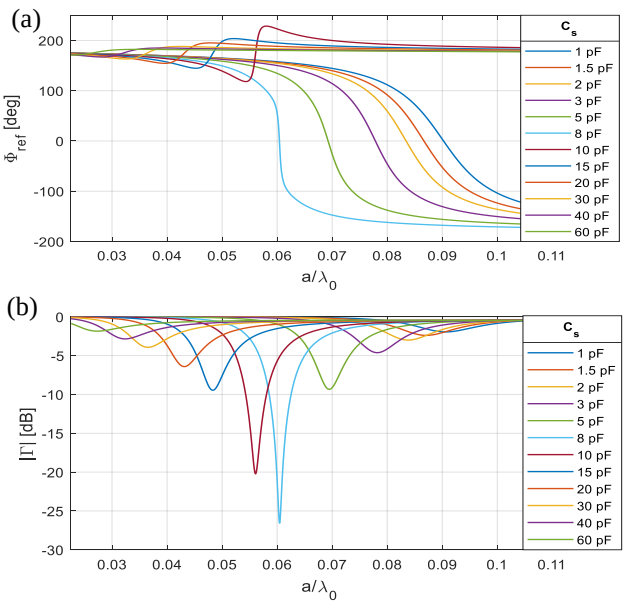

Fig. 5. Reflection coefficient for the square patch HIS with lossy additional capacitor (R_s = 10 Ω): (a) phase Φ_{ref} (b) magnitude |Γ|.

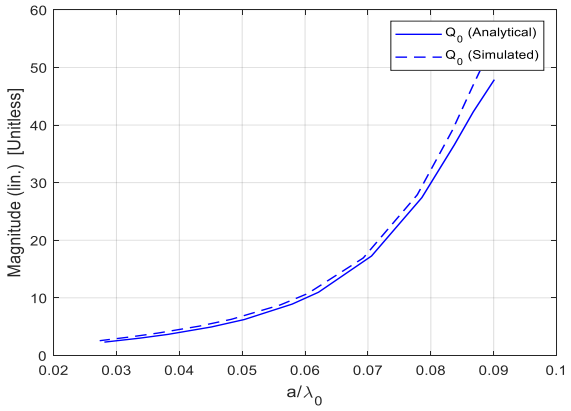

Fig. 6. Unloaded quality factor Q_0 between analitycal (blue) and simulated (red) results for the square patch HIS (R_s = 10 Ω).

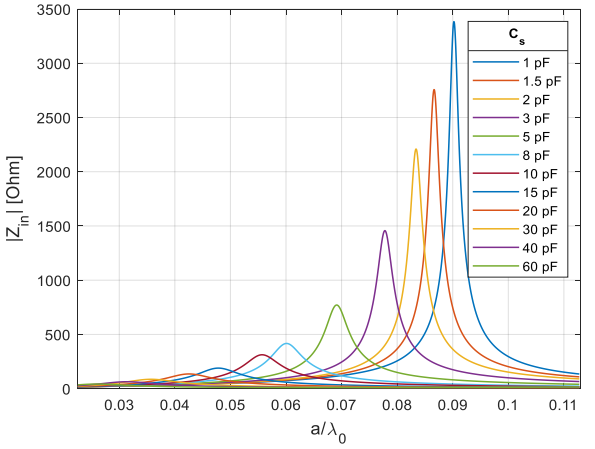

Fig. 7. Magnitude of the input impedance |Z_{in}| for the square patch HIS with lossy additional capacitor (R_s = 10 Ω).

IV. Unit Cells Comparison

In this section, the ratio between the unloaded quality factor Q_0 and the electrical length is applied to three different unit cell geometries. The approach is inspired by [5] where the performance of different HIS geometries are compared according to the *R* coefficient, which is the ratio between the HIS fractional bandwidth $FBW_{\pm90}$ in % and the unit cell surface in mm². In this reference, all the HIS are designed with the same substrate features (height, permittivity, loss tangent) and the variation of the unit cell size enables to reach the same operating frequency f_0. According to [5], the ranking regarding the *R* coefficient is as follows, in decreasing order: a 6-armed intertwined hexagonal spiral, a 4-armed intertwined square spiral and the previously seen square patch. For fair comparison with the proposed ratio, a modified *R* coefficient is defined by the ratio between the HIS bandwidth $FBW_{\pm90}$ and the unit cell electrical length.

In this paper, a capacitor C_s with its resistive part R_s is added in the unit cell to tune the frequency response of the metasurface. For the patch HIS, the capacitors are added between each patch, Fig. 8(a). For both spiral HIS, a microstrip line network with capacitors is designed behind the unit cell ground plane and connected to the metallic spiral by four conducting vias, without any electrical contact with the ground plane, Fig. 8(b)-(c) [18]. Comparison is made according to the unloaded quality factor Q_0, the reflection coefficient magnitude |Γ|, the modified *R*, and the criterion Q_0

over the unit cell electrical length, in the case of lossless and lossy capacitors. The operating frequency f_0 is reached by modifying the value of C_s, from 0.5 pF to 4 pF. The length a equals to 150.2mm, 33.94 mm, and 31.75 mm respectively for the square patch, the 4-armed intertwined square spiral and the 6-armed intertwined hexagonal spiral, respectively, Fig. 8. The size difference between square patch and 4-armed intertwined square spiral has already been observed in [19], because of the added transmission line network on the bottom side.

A. *Lossless capacitor case (R_s = 0 Ω)*

In the case of lossless capacitors, the ranking between unit cell geometries is the same when comparing the unloaded quality factor Q_0, the fractional bandwidth $FBW_{\pm 90}$ and the reflection coefficient magnitude |Γ|, Fig. 9, Fig. 10 and Fig. 11 respectively. The 6-armed hexagonal spiral has a lower |Γ| than the 4-armed square spiral and the square patch. The performance of the 6-armed hexagonal spiral and the 4-armed square spiral will be examined as they have the lowest electrical size. By taking into account the size of each unit cell in order to emphasize the unit cell performance depending on its compactness, the modified R coefficient indicates better performance for the 4-armed square spiral, Fig. 12 (~118% better). The criterion Q_0 over the unit cell electrical length also displays better performance for the 4-armed square spiral, Fig. 13 (~15% better). The difference is less important as intrinsic losses of the geometry are taken into account and shown on Fig. 10. Therefore, in the case of lossless capacitors and in free space environment, there is no interest in choosing the 6-armed hexagonal spiral for antenna design. However, while designing antenna for multi-functional applications, the resistive part of the additional lumped elements cannot be neglected as it can have a strong influence on the HIS performance.

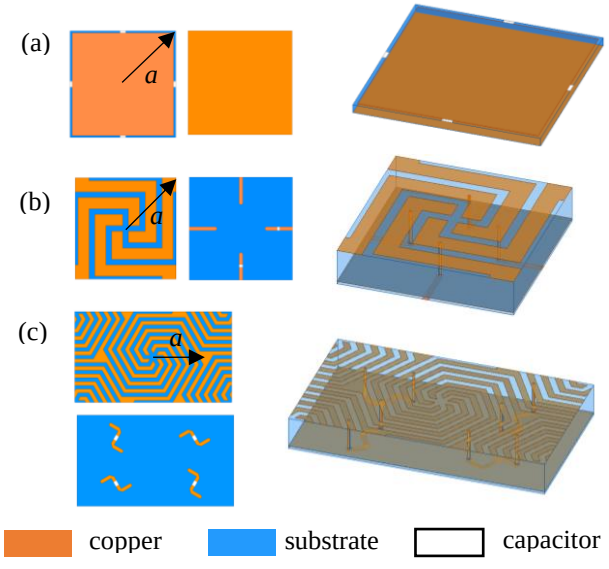

Fig. 8. Unit cells design with additional capacitors and a, the radius of the smallest hypothetical sphere enclosing the unit cell: (a) the patch (b) the 4-armed intertwined square spiral and (c) the 6-armed intertwined hexagonal spiral, with front view, back view and 3D view.

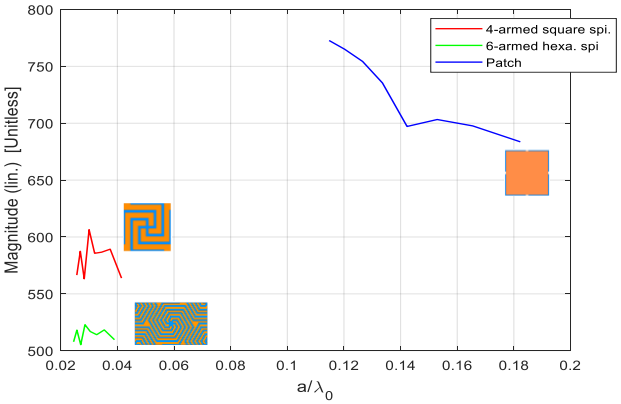

Fig. 9. Unloaded quality factor Q_0 for the 4-armed square spiral (red), 6-armed hexagonal spiral (green) and the patch HIS (blue), for lossless capacitors.

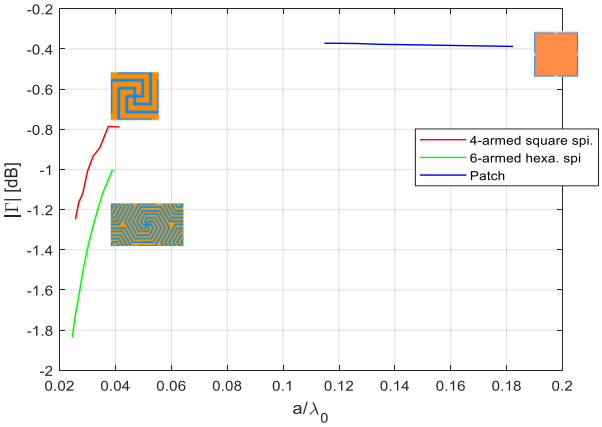

Fig. 10. Reflection coefficient magnitude |Γ| for the 4-armed square spiral (red), 6-armed hexagonal spiral (green) and the patch HIS (blue), for lossless capacitors.

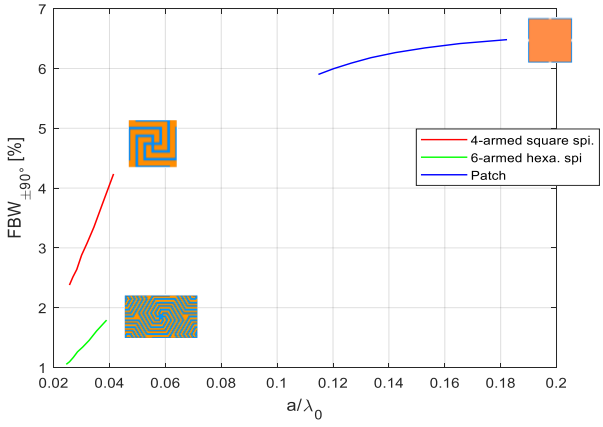

Fig. 11. Fractional bandwidth $FBW_{\pm 90}$ for the 4-armed square spiral (red), 6-armed hexagonal spiral (green) and the patch HIS (blue), for lossless capacitors.

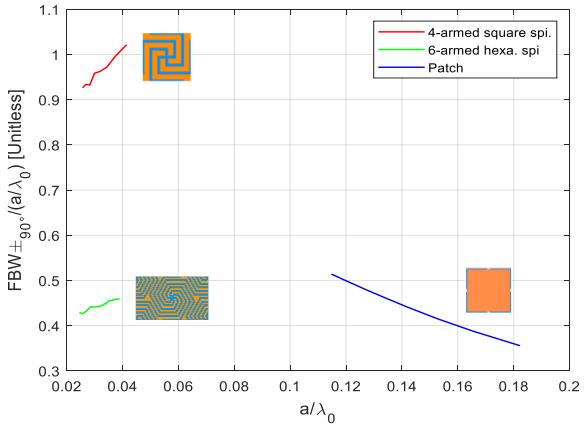

Fig. 12. Modified *R* coefficient for the 4-armed square spiral (red), 6-armed hexagonal spiral (green) and the patch HIS (blue), for lossless capacitors.

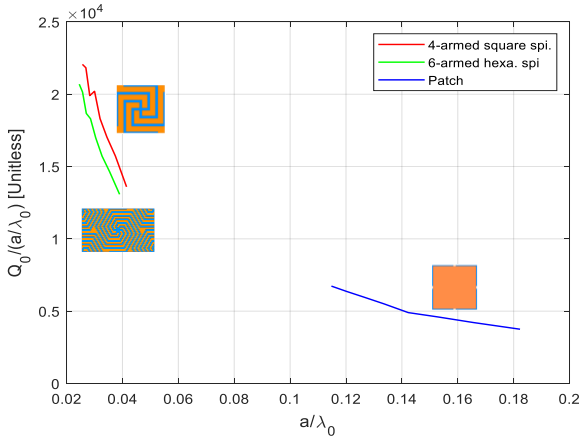

Fig. 13. Q_0 over the unit cell size for the 4-armed square spiral (red), 6-armed hexagonal spiral (green) and the patch HIS (blue), for lossless capacitors.

B. Lossy capacitor case (R_s = 5 Ω)

In this section, the performance of the patch unit cell will not be compared anymore as it has the highest electrical size. In the case of lossy capacitors, the ranking between unit cell geometries is the same when comparing the unloaded quality factor Q_0 and the reflection coefficient magnitude |Γ|, Fig. 14 and Fig. 15, before the swing phase zone proper to each unit cell. Unlike the lossless case, the 4-armed square spiral has a lower |Γ| than the 6-armed hexagonal spiral. The modified *R* coefficient is also different compared to the lossless case and the unit cell ranking depends on the unit cell electrical length size, Fig. 16. For a/λ_0>0.032, the modified *R* coefficient indicates better performance for the 4-armed square spiral (~9% better at a/λ_0=0.038), whereas, for a/λ_0<0.032, the 6-armed hexagonal spiral becomes better (~24% better at a/λ_0=0.029). Meanwhile, as the unloaded quality factor Q_0 also considers the losses inside a resonant circuit, the criterion Q_0 over the unit cell electrical length depicts better performance for the 6-armed hexagonal spiral (~151% better at a/λ_0=0.038 and ~35% better at a/λ_0=0.029), regardless the electrical length size, Fig. 17. Furthermore, the criterion Q_0 over the unit cell electrical length still exists for phase swing zone of each unit cell, a/λ_0<0.027 for the 4-armed square spiral and a/λ_0<0.025 for the 6-armed hexagonal spiral, Fig. 17. This is not the case for the modified *R* coefficient anymore, Fig. 16.

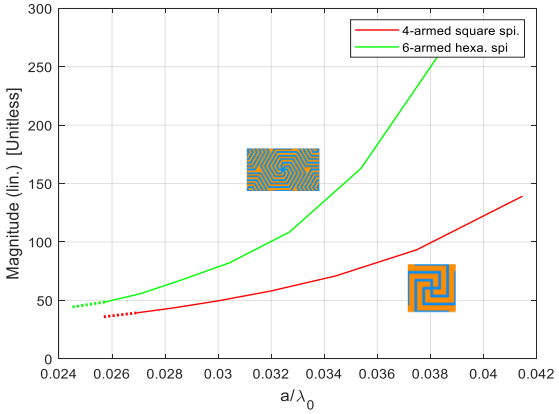

Fig. 14. Unloaded quality factor Q_0 for the 4-armed square spiral (red) and the 6-armed hexagonal spiral (green), for lossy capacitors. Dotted lines represent the phase swing zone for each unit cell.

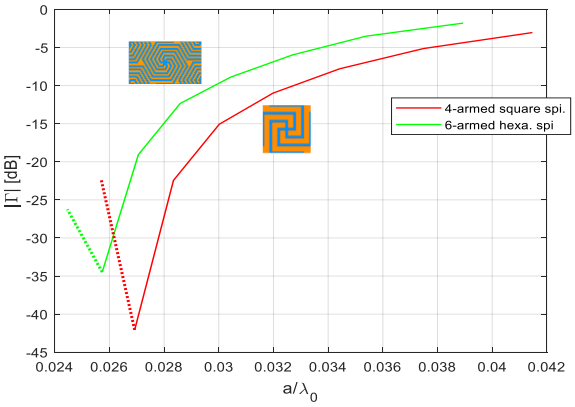

Fig. 15. Reflection coefficient magnitude |Γ| for the 4-armed square spiral (red) and the 6-armed hexagonal spiral (green), for lossy capacitors. Dotted lines represent the phase swing zone for each unit cell.

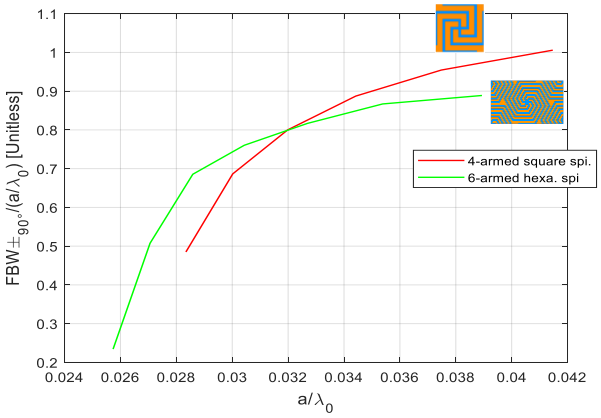

Fig. 16. Modified *R* coefficient for the 4-armed square spiral (red) and the 6-armed hexagonal spiral (green), for lossy capacitors.

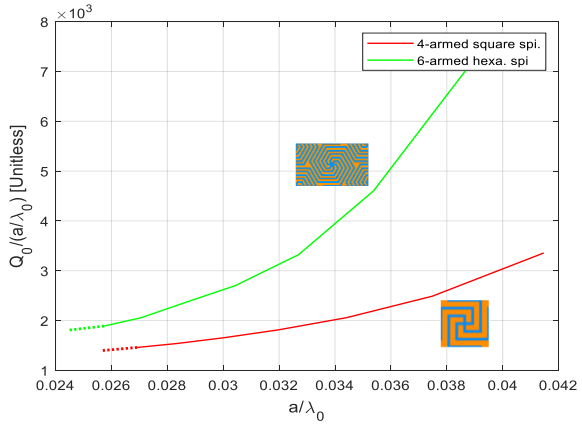

Fig. 17. Q_0 over the unit cell size for the 4-armed square spiral (red) and the 6-armed hexagonal spiral (green), for lossy capacitors. Dotted lines represent the phase swing zone for each unit cell.

V. Conclusion

When designing a tunable metasurface for multi-functional applications, the resistive part of components may not be negligible. Thus, the quality factor Q is assumed to be an adequate parameter to evaluate losses of a resonant circuit. The loaded quality factor $Q_{L,RLC}$ and the unloaded quality factor Q_0 of the square patch HIS with additional capacitors are examined. $Q_{L,RLC}$ of the HIS is compared to $Q_{L,\pm 90°} = 1/FBW_{\pm 90°}$, where $FBW_{\pm 90}$ is the fractional bandwidth of the infinite HIS. For lossless additional capacitors, $Q_{L,RLC}$ and $Q_{L,\pm 90°}$ follow the same trend. But, for lossy capacitors, the evolutions of $Q_{L,RLC}$ and $Q_{L,\pm 90°}$ diverge. Therefore, $Q_{L,RLC}$ is not only related to $FBW_{\pm 90}$ but it also takes into account the influence of additional losses. As $Q_{L,RLC}$ depends on the unit cell environment, the unloaded quality factor Q_0 is proposed to analyze different unit cells with additional capacitors.

The performance of different HIS geometries are compared according to the criterion Q_0 over the unit cell electrical length and the modified R coefficient inspired by [5], which is the ratio between the HIS fractional bandwidth $FBW_{\pm 90}$ in % and the unit cell electrical length. The geometries under study are the 4-armed intertwined square spiral and the 6-armed intertwined hexagonal spiral. For lossless additional capacitors, the 4-armed intertwined square spiral exhibits better performance compared to the 6-armed intertwined hexagonal spiral according to the modified R coefficient (~118% better) and the criterion Q_0 over the unit cell electrical length (~15% better). Meanwhile, for lossy additional capacitors, the 6-armed intertwined hexagonal spiral exhibits better performance (~151% better at a/λ_0=0.038 and ~35% better at a/λ_0=0.029) according to the proposed criterion, whereas the unit cells ranking by the modified R coefficient depends on the electrical length size. It indicates ~9% better performance for the 4-armed square spiral at a/λ_0=0.038, whereas, the 6-armed hexagonal spiral becomes ~24% better at a/λ_0=0.029. While the modified R coefficient highlights wideband and/or compact unit cells, the unloaded quality factor Q_0 also considers the loss inside a resonant circuit. Furthermore, this criterion still exists for phase swing zone that may appear for small electrical length unit cell, and thus compact unit cell. That is not the case with the modified R coefficient. Therefore, for a HIS in free space environment, the 6-armed intertwined hexagonal spiral can be considered to design compact multi-functional antennas with a lower reflection coefficient magnitude |Γ|.

References

[1] D. Sievenpiper, “High-impedance electromagnetic surfaces,” Ph.D. dissertation, Dept. Elect. Eng., Univ. California at Los Angeles, Los Angeles, CA, 1999.

[2] F. Costa, S. Genovesi and A. Monorchio, "On the Bandwidth of High-Impedance Frequency Selective Surfaces," in IEEE Antennas and Wireless Propagation Letters, vol. 8, pp. 1341-1344, 2009, doi: 10.1109/LAWP.2009.2038346.

[3] S. B. Glybovski, S. A. Tretyakov, P. A. Belov, Y. S. Kivshar, and C. R. Simovski, ‘Metasurfaces: From microwaves to visible’, Physics Reports, vol. 634, pp. 1–72, May 2016, doi: 10.1016/j.physrep.2016.04.004.

[4] C. P. Scarborough and al., ‘Compact Low-Profile Tunable Metasurface-Enabled Antenna With Near-Arbitrary Polarization’, in IEEE Transactions on Antennas and Propagation, vol. 64, no. 7, pp. 2775-2783, July 2016.

[5] A. Bellion and M. Cable, ‘A new wideband and compact High Impedance Surface’, 2012 15 International Symposium on Antenna Technology and Applied Electromagnetics, pp. 1-5, 2012.

[6] A. Li, Z. Luo, H. Wakatsuchi, S. Kim, et D. F. Sievenpiper, « Nonlinear, Active, and Tunable Metasurfaces for Advanced Electromagnetics Applications », IEEE Access, vol. 5, p. 27439-27452, 2017, doi: 10.1109/ACCESS.2017.2776291.

[7] S. Kim, A. Li, J. Lee and D. F. Sievenpiper, "Active Self-Tuning Metasurface With Enhanced Absorbing Frequency Range for Suppression of High-Power Surface Currents," in IEEE Transactions on Antennas and Propagation, vol. 69, no. 5, pp. 2759-2767, May 2021, doi: 10.1109/TAP.2020.3032834.

[8] Ratni, B., de Lustrac, A., Piau, GP. et al. Active metasurface for reconfigurable reflectors. Appl. Phys. A 124, 104 (2018). https://doi.org/10.1007/s00339-017-1502-4

[9] D. Chen, W. Yang, W. Che, Q. Xue and L. Gu, "Polarization-Reconfigurable and Frequency-Tunable Dipole Antenna Using Active AMC Structures," in IEEE Access, vol. 7, pp. 77792-77803, 2019, doi: 10.1109/ACCESS.2019.2919518.

[10] S. A. Tretyakov and C. R. Simovski, ‘Dynamic Model of Artificial Reactive Impedance Surfaces’, Journal of Electromagnetic Waves and Applications, vol. 17, no. 1, pp. 131–145, Jan. 2003.

[11] D. Pozar, *Microwave Engineering.* Wiley, 2012.

[12] S. A. Cummer, B. Popa and T. H. Hand, "Q-Based Design Equations and Loss Limits for Resonant Metamaterials and Experimental Validation," in IEEE Transactions on Antennas and Propagation, vol. 56, no. 1, pp. 127-132, Jan. 2008, doi: 10.1109/TAP.2007.912959.

[13] S. Pan, C. Guclu and F. Capolino, "Effect of losses on the performance of very thin artificial magnetic conductors," 2013 International Symposium on Electromagnetic Theory, 2013, pp. 404-407.

[14] J. J. Sanz-Fernandez, R. Cheung, G. Goussetis and C. Mateo-Segura, "Power Stored and Quality Factors in Frequency Selective Surfaces at THz Frequencies," in IEEE Transactions on Antennas and Propagation, vol. 59, no. 6, pp. 2205-2216, June 2011, doi: 10.1109/TAP.2011.2143654.

[15] K. K. Karnati, Y. Yusuf, S. Ebadi and X. Gong, "Theoretical Analysis on Reflection Properties of Reflectarray Unit Cells Using Quality Factors," in IEEE Transactions on Antennas and Propagation, vol. 61, no. 1, pp. 201-210, Jan. 2013, doi: 10.1109/TAP.2012.2214753.

[16] H. Mosallaei and K. Sarabandi, "Antenna miniaturization and bandwidth enhancement using a reactive impedance substrate," in IEEE Transactions on Antennas and Propagation, vol. 52, no. 9, pp. 2403-2414, Sept. 2004.

[17] ANSYS, HFSS Help - Release 2021 R1 (User Guide). Canonsburg: ANSYS, 2021.

[18] N. Kristou, J. Pintos and K. Mahdjoubi, "Miniaturized tunable artificial magnetic conductor for low LTE band," 2017 IEEE International Symposium on Antennas and Propagation & USNC/URSI National Radio Science Meeting, 2017, pp. 461-462, doi: 10.1109/APUSNCURSINRSM.2017.8072273.

[19] N. Kristou, J. -F. Pintos and K. Mahdjoubi, "Low profile dipole antenna over compact AMC surface," 2017 International Workshop on Antenna Technology: Small Antennas, Innovative Structures, and Applications (iWAT), 2017, pp. 64-67, doi: 10.1109/IWAT.2017.7915318.